

# Discovery of Novel Binders to Sterol Regulatory Element-Binding Protein-1 by High-Throughput Screening

Takashi Maruyama,<sup>#</sup> Yu Takahashi,<sup>\*,#</sup> Kahori Hiro, Kohji Murase, Hirotatsu Kojima, Takayoshi Okabe, Yoshio Yamauchi, and Ryuichiro Sato<sup>\*</sup>



Cite This: *ACS Med. Chem. Lett.* 2024, 15, 667–676



Read Online

ACCESS |

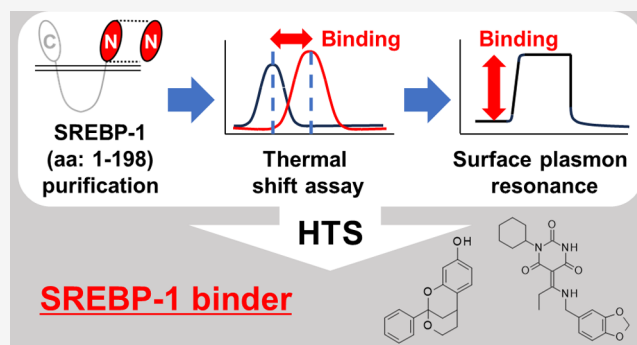
Metrics & More

Article Recommendations

Supporting Information

**ABSTRACT:** Sterol regulatory element-binding protein-1 (SREBP-1) is a transcription factor that regulates the expression of genes related to fatty acid biosynthesis. Its high expression and activation in obesity and associated metabolic diseases make it a potential therapeutic target. However, the role of SREBP-1 in the development and exacerbation of these diseases remains unclear, partly because of the impossibility of inhibiting its function because of the lack of specific inhibitors. Here, we aimed to identify small-molecule compounds that directly bind to SREBP-1 using the recombinant N-terminal region of SREBP-1a, which is required for its transcriptional activity. A high-throughput screening campaign was conducted using a thermal shift assay and surface plasmon resonance assay to evaluate the compound affinity and specificity, which resulted in the identification of two compounds. Future analysis of their structure–activity relationships may lead to the development of specific SREBP-1 inhibitors, thereby potentially validating SREBP-1 as a therapeutic target for obesity and resultant atherosclerotic diseases.

**KEYWORDS:** Sterol Regulatory Element-Binding Protein-1, Protein Purification, High-throughput Screening, Binder, Thermal Shift Assay, Surface Plasmon Resonance



The number of individuals with metabolic disorders, such as obesity, dyslipidemia, and type II diabetes, has been increasing. The primary reason for the development of these diseases is disruption of lipid homeostasis.<sup>1</sup> Sterol regulatory element-binding protein (SREBP)-1 is a crucial transcription factor that is activated upon feeding and regulates the expression of enzymes involved in fatty acid biosynthesis.<sup>2,3</sup> In obese mouse models, SREBP-1 is overexpressed and activated, which leads to fatty liver, insulin resistance, and dyslipidemia.<sup>4</sup> These findings suggest that excessive SREBP-1 activation contributes to the onset or worsening of metabolic disease. However, it remains unknown whether SREBP-1 is a target molecule for disease prevention and treatment, partly because SREBP-1-deficient mice exhibit compensatory activation of SREBP-2, which belongs to the same family and regulates the expression of cholesterol biosynthetic enzymes.<sup>5</sup> SREBPs are localized in the endoplasmic reticulum as inactive precursors by forming complexes with SREBP cleavage-activating protein (SCAP) and insulin-induced gene proteins (INSIGs).<sup>6</sup> Upon external stimuli, such as cholesterol depletion in the ER membrane, the SREBP-SCAP complex is transported to the Golgi apparatus, where SREBPs are sequentially cleaved by site-1 and site-2 proteases and the released N-terminal domain enters the nucleus to activate

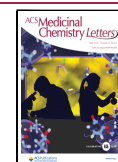
transcription. Cholesterol and oxysterol bind to SCAP and INSIGs, respectively, and stabilize the SCAP–INSIG interaction to retain SREBPs in the ER.<sup>7</sup> Several small-molecule inhibitors have been reported to prevent SREBP activation. For example, fatostatin and betulin bind to SCAP, and enhance SCAP–INSIG interactions, and lycorin enhances the degradation of SCAP, thereby inhibiting SREBPs translocation to the Golgi apparatus.<sup>8–10</sup> However, these inhibitors act on the machinery that activates both SREBP-1 and SREBP-2, and no specific inhibitors of SREBP-1 or SREBP-2 have been reported to date. Considering that brain-specific SCAP-deficient mice exhibit decreased cholesterol synthesis in the brain, as well as impaired synaptic transmission and cognitive function,<sup>11</sup> long-term SREBP-2 inhibition, especially in the brain, might lead to undesirable side effects. Therefore, the development of SREBP-1-specific inhibitors is especially desirable to under-

**Received:** February 6, 2024

**Revised:** March 26, 2024

**Accepted:** April 11, 2024

**Published:** April 17, 2024



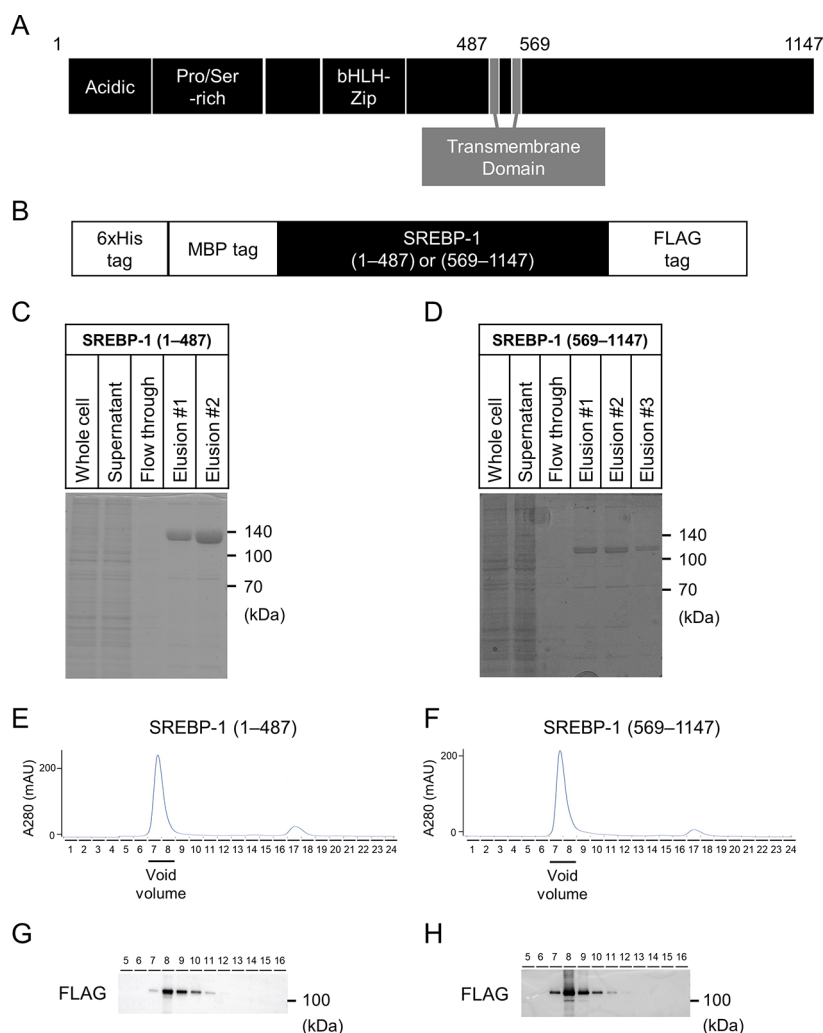


**Figure 1.** Expression and purification of N- and C-terminal cytosolic human SREBP-1a in Sf9 insect cells. (A,B) Schematic representation of the domain structure of human SREBP-1a, namely acidic, Ser/Pro-rich, basic helix–loop–helix leucine zipper (bHLH-Zip), and transmembrane domains. For recombinant protein expression, a 6 × His-MBP tag and a FLAG tag were attached to the N- and C-termini, respectively. (C,D) After 24 h of infection with a baculovirus for SREBP-1a (1–487 or 569–1147) expression, Sf9 cells cultured on a 200 mL culture scale were harvested. Cell lysates were purified on an anti-FLAG antibody affinity gel. The first elution fraction was prepared by adding 1 mL of elution buffer containing 150 μg/mL 3xFLAG peptide. The next elution fraction was prepared by adding 1 mL of buffer containing 150 μg/mL 3xFLAG peptide in the same manner after the elution of the previous fraction was completed. This process was repeated to obtain the elution fractions. Each elution fraction was regarded as concentrated 200-fold compared with that of the supernatant. Equal volumes of each sample were subjected to SDS-PAGE followed by CBB staining. (E,F) Total elution fractions were analyzed by size-exclusion chromatography by determining the absorbance at 280 nm (A280). The numbers indicate each fraction. (G,H) Equal volumes of each fraction, including the peak, were subjected to SDS-PAGE and immunoblotting with an anti-FLAG antibody.

stand metabolic disease progression and establish disease treatment strategies.

SREBP-1, a double-pass transmembrane protein, exists as two isoforms: SREBP-1a and SREBP-1c. The SREBP-1a isoform is characterized by an additional 24 amino acid residues at the N-terminus compared with SREBP-1c, which contributes to its higher transcriptional activity than that of SREBP-1c.<sup>12</sup>

In this study, we purified the N-terminal region of human SREBP-1a and used it as a tool to screen for small-molecule binders of SREBP-1a from a large chemical library. Primary screening was conducted using a thermal shift assay (TSA), which allows high-throughput evaluation of the effect of compound binding on the thermal stability of the protein.<sup>13</sup> Subsequently, surface plasmon resonance (SPR) was per-

formed to assess the affinity and specificity of compound,<sup>14</sup> and two were selected as potential hits.

For the identification of direct binders to human SREBP-1, we aimed to obtain purified recombinant human SREBP-1. However, membrane proteins, such as SREBP-1, which possess two transmembrane regions, are prone to aggregation and require solubilization with detergents or expression with specialized materials, such as nanodiscs, for biochemical assays.<sup>15,16</sup> Furthermore, there have been no reports of the purification of mammalian SREBP-1. Therefore, we first attempted to express and purify the cytosolic N-terminal (1–487) and C-terminal (569–1147) regions of SREBP-1a using a baculovirus–insect cell expression system (Figure 1A), which is considered more suitable for expressing recombinant proteins with high molecular weights than *Escherichia coli*.<sup>17</sup> To enhance protein solubility, we added a hexahistidine (6 ×

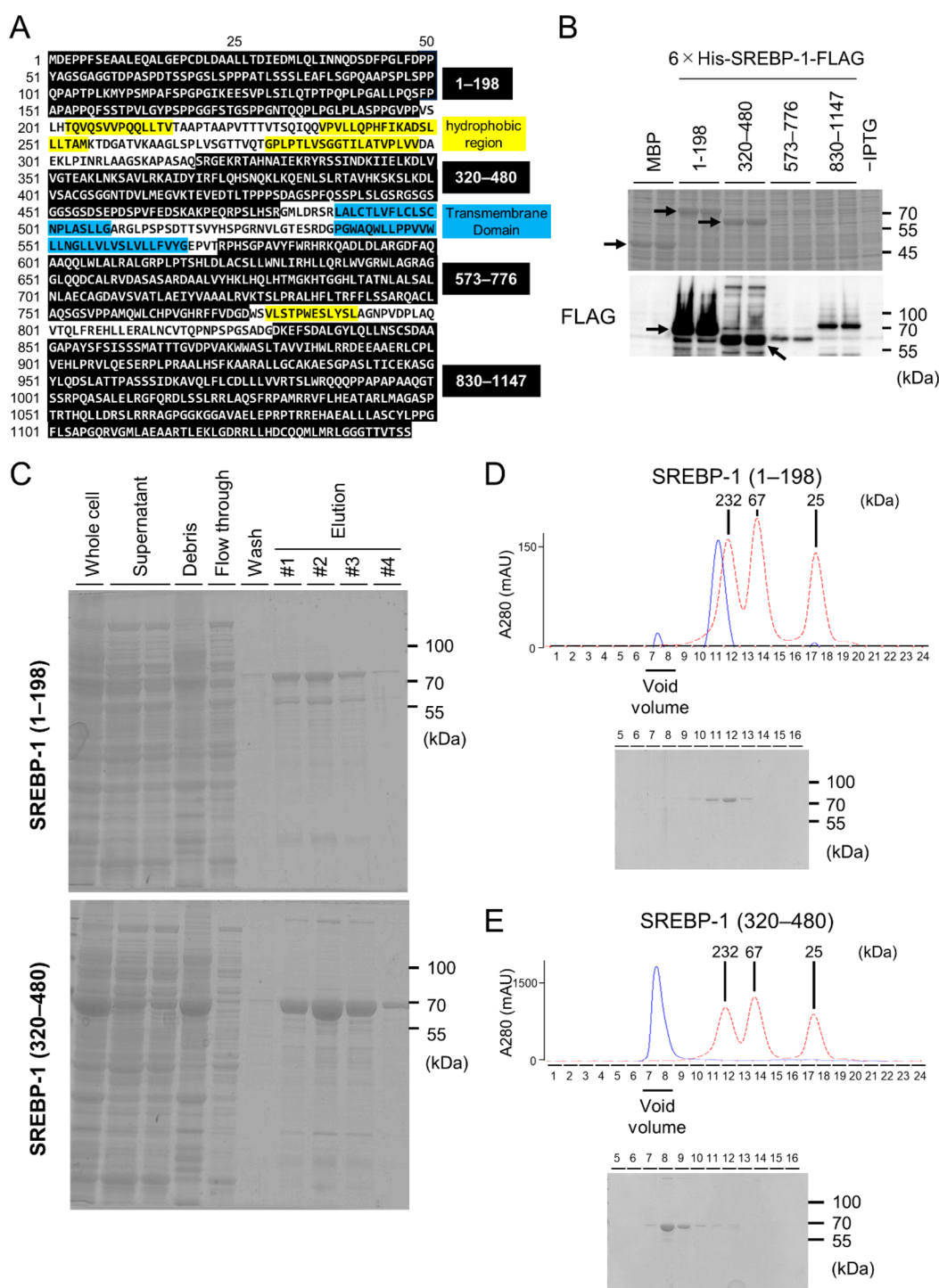


**Figure 2.** Expression and purification of divided SREBP-1a regions in *E. coli* BL21 (DE3) cells. (A) Amino acid sequence analysis of human SREBP-1a using PSIPRED and each divided region for protein purification, excluding predicted hydrophobic regions (yellow, 203–226, 236–255, 279–298, 779–790 AAs) and transmembrane domains (blue, 488–508, 538–568 AAs). (B) *E. coli* BL21 (DE3) cells transformed with SREBP-1 expression plasmids were harvested and sonicated, and the supernatant was subjected to SDS-PAGE followed by CBB staining (upper panel) or immunoblotting with an anti-FLAG antibody (lower panel). Samples for each lane were prepared from different colonies of *E. coli* BL21 (DE3) after transformation. The arrows indicate bands of the target proteins. (C) The cell lysate prepared from BL21 (DE3) cells cultured on a 50 mL culture scale was purified using an anti-FLAG antibody affinity gel. The first elution fraction was prepared by adding 1 mL of elution buffer containing 150  $\mu\text{g}/\text{mL}$  3xFLAG peptide. The next elution fraction was prepared by adding 1 mL of buffer containing 150  $\mu\text{g}/\text{mL}$  3xFLAG peptide in the same manner after the elution of the previous fraction was completed. The process was repeated to obtain the elution fractions. Each elution fraction was regarded as concentrated 50-fold compared with that of the supernatant. Equal volumes of each sample were subjected to SDS-PAGE followed by CBB staining. (D,E) Total elution fractions were analyzed by size-exclusion chromatography by determining the absorbance at 280 nm. The red dotted line represents the molecular weight markers of 25, 67, and 232 kDa. Equal volumes of each fraction were subjected to SDS-PAGE followed by CBB staining.

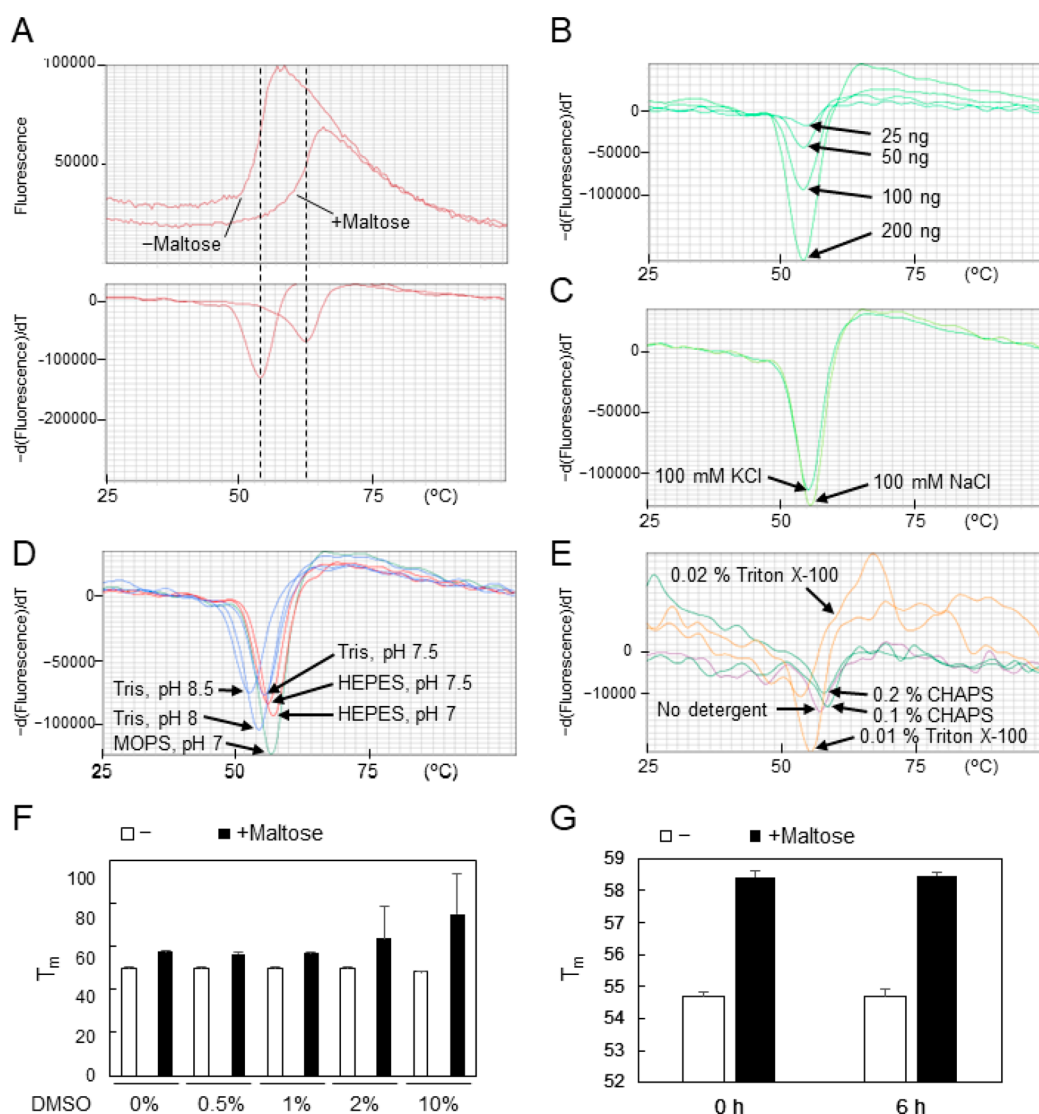


**Figure 3.** Optimization of TSA for SREBP-1 binder screening. (A) A representative melting curve (upper panel) or its differential curve (lower panel) of 100 ng of purified 6 × HisMBP-SREBP-1 (1–198) in assay buffer (20 mM Tris, pH 8, and 100 mM NaCl) in the presence or absence of 1 mM maltose. The dotted lines indicate  $T_m$ . (B) Differential melt curves of 25, 50, 100, or 200 ng of purified 6 × HisMBP-SREBP-1a (1–198) in assay buffer (20 mM Tris, pH 8, and 100 mM NaCl). (C) Differential melt curves of 100 ng of purified 6 × HisMBP-SREBP-1a (1–198) in 50 mM MOPS, pH 7, in the presence of 100 mM NaCl or 100 mM KCl. (D) Differential melt curves of 100 ng of purified 6 × HisMBP-SREBP-1a (1–198) in various buffers indicated in the graph in the presence of 100 mM NaCl. Tris, MOPS, and HEPES buffers are denoted by blue, green, and red, respectively. (E) Differential melt curves of 100 ng of purified 6 × HisMBP-SREBP-1a (1–198) in assay buffer (50 mM MOPS, pH 7, and 100 mM NaCl) in the presence or absence of Triton X-100 (0.01%, 0.02%) or CHAPS (0.1%, 0.2%). (F) The effect of DMSO concentration on  $T_m$  values of 200 ng of purified 6 × HisMBP-SREBP-1 (1–198) in TSA buffer (50 mM MOPS, pH 7, 100 mM NaCl, 0.01% Triton X-100). Data represent mean  $\pm$  SD ( $n = 5$ ). (G) Change in  $T_m$  values in the presence or absence of maltose immediately (0 h) or 6 h after preparation of protein solution mixtures in TSA buffer. Data represent mean  $\pm$  SD (– maltose,  $n = 48$ ; + maltose,  $n = 16$ ).

His)-maltose-binding protein (MBP) tag at the N-terminus<sup>18</sup> and a FLAG tag at the C-terminus for affinity purification (Figure 1B). The baculovirus-expressing MBP-tagged SREBP-1a was prepared in Sf9 insect cells by using a bacmagen transfection kit. After the amplification of viruses by repetitive infection of Sf9 cells, the virus was used to infect Sf9 cells for 24 h. After harvesting, sonication, and centrifugation of the cells at 100 000 g for 2 h, the supernatant was collected and purified using an anti-FLAG antibody. Each elution fraction was prepared sequentially by competitive elution with FLAG peptides with the next elution proceeding after the previous elution was completed. Although both regions of overexpressed SREBP-1a were clearly observed in the elution

fractions by Coomassie brilliant blue (CBB) staining (Figure 1C,D), size-exclusion chromatography revealed that almost all of the proteins were eluted in the void volume (Figure 1E,F), which was further confirmed by immunoblotting (Figure 1G,H). Considering the separation ability of the Superdex200 10/30 GL column used, the result suggested that the protein particle size was much larger than the expected molecular size, and one possible cause of this could be the formation of protein aggregates. Thus, we concluded that the cytosolic N-terminal (1–487) and C-terminal (569–1147) regions of SREBP-1a are difficult to purify with their protein structure being kept in a natural state.

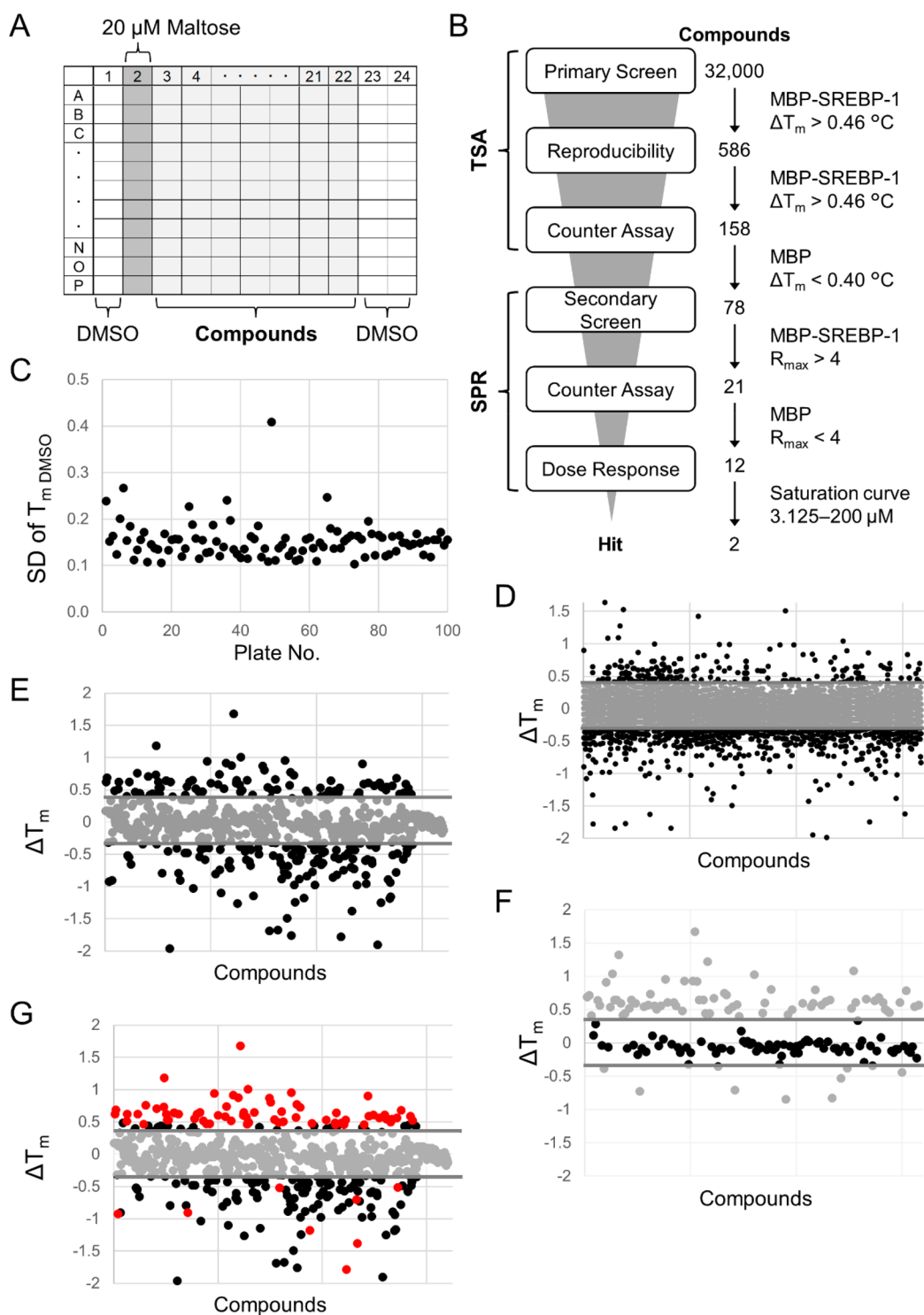


**Figure 4.** High-throughput SREBP-1 binder screening using TSA. (A) 384-well plate layout for the binder screens. Columns 1, 23, and 24 did not contain compounds (DMSO group), column 2 contained maltose at a final concentration of 20  $\mu\text{M}$ , and columns 3–22 contained compounds at a final concentration of 20  $\mu\text{M}$ . (B) Flowchart and summary of the screening campaign toward hit identification. (C) The average SD of the  $T_m$  values in each plate of the DMSO group in the primary screen was calculated and represented as a scatter plot. (D) For the 32 000 compounds evaluated in the primary screen,  $\Delta T_m$  was calculated and represented as a scatter plot. A total of 586 compounds with  $\Delta T_m$  greater than 0.46  $^{\circ}\text{C}$ , a statistical cutoff of  $3 \times \text{SD}$  of the DMSO groups, were selected. (E) Reproducibility tests for 586 compounds were performed under the same conditions using  $6 \times \text{HisMBP-SREBP-1a}$  (1–198) in quadruplicate, and the average  $\Delta T_m$  was plotted. A total of 158 compounds with  $\Delta T_m$  greater than 0.46  $^{\circ}\text{C}$ , a statistical cutoff of  $3 \times \text{SD}$  of the DMSO groups, were selected. (F) A counter assay for 158 compounds was performed in quadruplicate using purified  $6 \times \text{HisMBP}$  under the same conditions as those in the primary screening, and the average  $\Delta T_m$  was plotted. A total of 78 compounds with  $\Delta T_m$  less than 0.40  $^{\circ}\text{C}$ , a statistical cutoff of  $3 \times \text{SD}$  of the DMSO groups, were selected. (G) The compounds shown in Figure 4E, which were excluded from the counter assay in Figure 4F, are highlighted in red.

Considering the instability of the cytosolic regions of human SREBP-1a, we attempted to identify the hydrophobic amino acid-rich regions of the protein that might be responsible for aggregation using the PSIPRED Protein Analysis Workbench, which can predict a diverse suite of proteins and provide annotation tools focused principally on protein structures.<sup>19</sup> As illustrated in Figure 2A, we identified multiple regions containing many hydrophobic amino acids (AAs) in full-length human SREBP-1a. Consequently, we divided SREBP-1a into four domains (1–198, 320–480, 573–776, and 830–1147 AAs), excluding these regions (Figure 2A). Each region was deemed small enough to be expressed in *E. coli*, even though an MBP tag (43 kDa) was attached. *E. coli* BL21 (DE3) cells transformed with the expression plasmid were treated with isopropyl  $\beta$ -D-thiogalactopyranoside (IPTG) when the OD<sub>600</sub> reached 0.6, cultured for 24 h at 18 °C, and harvested. The cell pellets were sonicated and centrifuged at 100 000 g for 2 h, and the supernatant was collected. Because the region 1–198 and 320–480 AAs were found to be highly expressed in *E. coli* by CBB staining and immunoblotting (Figure 2B), each protein was purified using anti-FLAG antibody affinity chromatography (Figure 2C). As shown in Figure 1C,D, each elution fraction was prepared sequentially by competitive elution with FLAG peptides, with the next elution proceeding after the previous elution was completed. The fractions were then subjected to secondary size-exclusion chromatography. In the region of 1–198 AA, the chromatogram showed a single peak in the column volume (Figure 2D). The obtained protein was larger than the expected molecular weight, which suggested that SREBP-1 (1–198) formed a multimer. This observation is consistent with a previous report showing that the N-terminal region of SREBP-1 forms dimers.<sup>20</sup> In contrast, 6  $\times$  HisMBP-SREBP-1a (320–480) was eluted from the void volume (Figure 2E), which suggested that this region was not sufficiently stable to be obtained as a properly folded, purified protein. On the basis of these results, we conclude that recombinant SREBP-1a (1–198) can be prepared on a large scale using the two-step purification approach, thereby enabling high-throughput screening (HTS) to identify SREBP-1a binders. To our knowledge, this is the first report to purify human SREBP-1a, which would contribute not only to screening studies but also to X-ray crystallography for protein structural analysis in the future. In addition, as for SREBP-1 (320–480) expressed in *E. coli* and SREBP-1 (1–487) and SREBP-1 (569–1147) expressed in the baculovirus–insect cell expression system, it would be intriguing to investigate whether refolding can be induced by denaturing agents, such as urea and guanidine–HCl, and/or reducing agents, such as  $\beta$ -mercaptoethanol and dithiothreitol, to obtain the appropriate conformation.

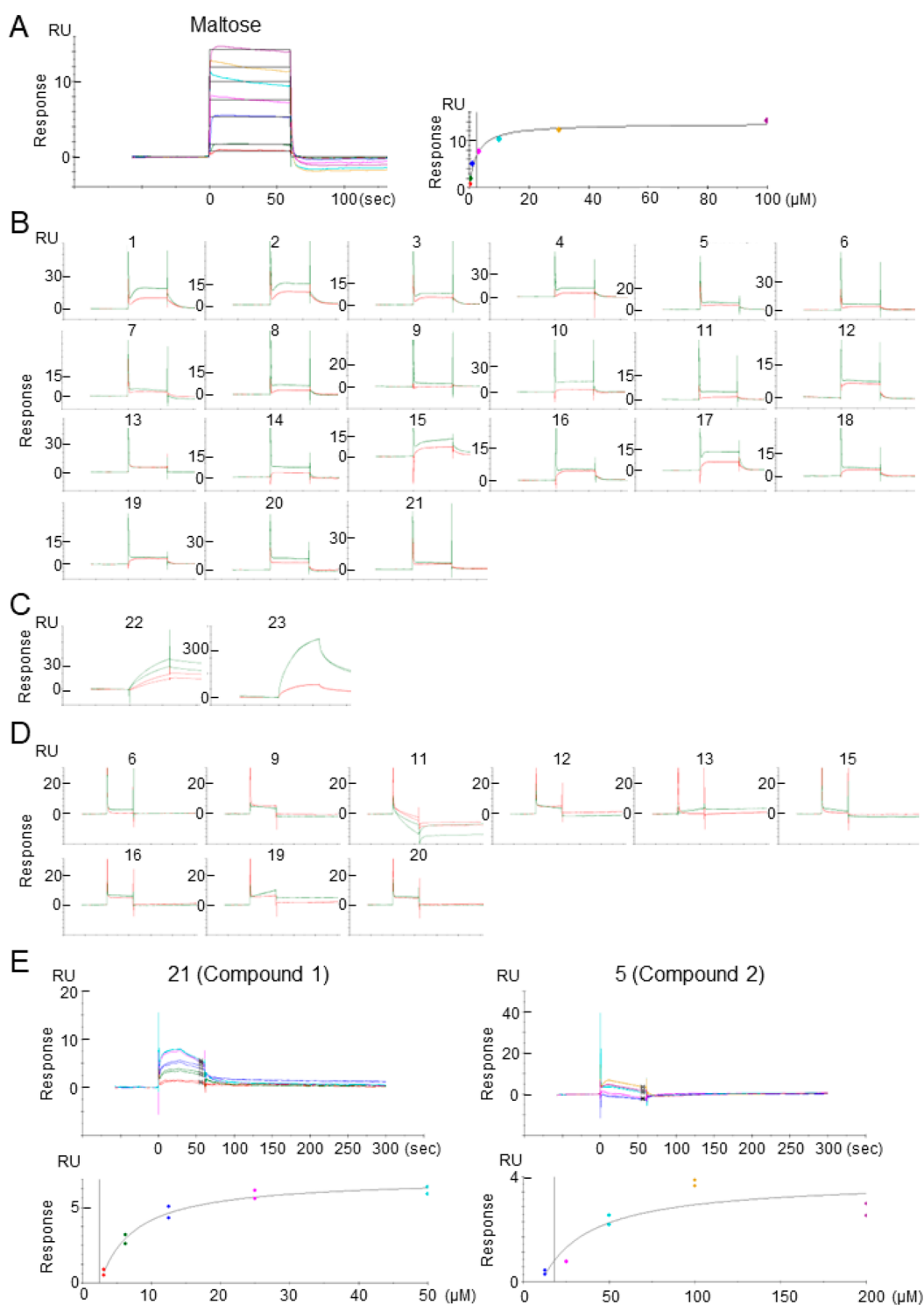
We conducted TSA to screen SREBP-1a binders with purified 6  $\times$  HisMBP-SREBP1a (1–198), as TSA is a highly efficient and cost-effective method for evaluating the binding capacity of compounds.<sup>21</sup> By determining the thermal melting curves (i.e., temperature denaturation curves) of 6  $\times$  HisMBP-SREBP-1a (1–198) by monitoring the fluorescent signals of SYPRO Orange, which binds to hydrophobic regions exposed during protein denaturation,<sup>22</sup> we confirmed an increase in the melting temperature ( $T_m$ ) from 54.1 to 62.6 °C upon the addition of maltose, which can bind to MBP (Figure 3A). These results indicated that purified 6  $\times$  HisMBP-SREBP-1a (1–198) is structurally stable and appropriate for TSA. On the basis of these results, we optimized the assay conditions,

including protein amounts and buffer components, by melting curve analysis. We observed a purified SREBP-1 dose-dependent increase in peak height in the differential melting curves (Figure 3B), thereby indicating that 100 ng is sufficient for binder evaluation. We found that 100 mM NaCl exhibited a slightly higher peak than that of 100 mM KCl (Figure 3C). We also found that the use of 50 mM Tris, pH 8, or 50 mM MOPS, pH 7, resulted in a peak higher than that of the other buffers in the differential melting curves (Figure 3D). Since SYPRO Orange also binds to detergents, which increases the background signal,<sup>22</sup> the addition of detergents may make it difficult to detect signal induction associated with protein thermal denaturation. However, detergents can inhibit non-specific binding to proteins; therefore, we examined whether any detergent can be added to TSA and found that the presence of 0.01% Triton X-100 had only a small effect on the signal compared with 0.02% Triton X-100, 0.1% CHAPS, and 0.2% CHAPS (Figure 3E). Furthermore, we adopted a 1% DMSO concentration for compound screening as the  $T_m$  value was not significantly affected by DMSO concentrations of up to 1% (Figure 3F). We also confirmed that the  $T_m$  and  $T_m$  shift values ( $\Delta T_m$ ) in response to maltose were hardly affected by incubation of the protein solution mixtures at room temperature for 6 h (Figure 3G), which indicated that the assay facilitates HTS. In conclusion, we determined an assay buffer consisting of 50 mM MOPS, pH 7, 100 mM NaCl, 0.01% Triton X-100, and 1% DMSO to carry out subsequent HTS.

We consider it important not to remove the MBP tag after purifying SREBP-1a to sustain its solubility,<sup>18</sup> although inclusion of the tag may increase the number of false positive hits as MBP binders. On the basis of the optimized assay conditions described previously, we developed TSA to perform HTS in a 384-well plate, as depicted in Figure 4A. Maltose was added to the second row as a positive control to ensure the  $T_m$  shift. The mean  $T_m$  value of the entire well in the absence of maltose was 54.7 °C with a standard deviation (SD) of 0.11 °C, which indicated interwell variability. However, the  $\Delta T_m$  in response to maltose was 3.73 °C, which was significantly greater than the SD in the DMSO group, which implied that the assay was robust enough for HTS.

Compound screening was carried out according to the flowchart shown in Figure 4B. Primary screening was conducted using TSA with a chemical library of small-molecule compounds at a final concentration of 20  $\mu$ M. The average SD of  $T_m$  values in the DMSO control group across all plates was 0.152 °C (Figure 4C). A total of 586 compounds with  $\Delta T_m > 0.46$  °C, which was the statistical cutoff (3  $\times$  SD) for the control group, were selected as primary hits from approximately 32 000 compounds (Figure 4D). Subsequently, a reproducibility test was performed in quadruplicate, and 158 compounds with  $\Delta T_m > 0.46$  °C (3  $\times$  SD) were selected (Figure 4E). As the  $T_m$  shift could also be induced by compounds binding to the tag regions, a counter assay was performed using purified 6  $\times$  HisMBP-FLAG under the same conditions as in the primary screening. Consequently, compounds with  $\Delta T_m > 0.40$  °C (3  $\times$  SD) were excluded as false hits, which resulted in the selection of 78 compounds (Figure 4F).

In a previous study, TSA of the MBP-tagged protein exhibited two peaks of melt curves originating from either the MBP tag or the target protein, thereby indicating that the MBP tag exists as an independent domain.<sup>23</sup> In this study, 6  $\times$  HisMBP-SREBP-1a (1–198) appeared to represent a single

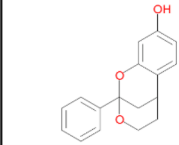
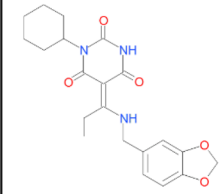


**Figure 5.** Identification of SREBP-1 binders with SPR. (A) Left panel: SPR sensorgram showing dose-dependent binding of maltose (0.1, 0.3, 1, 3, 10, 30, and 100  $\mu\text{M}$ ) to immobilized 6  $\times$  HisMBP-SREBP-1a (1–198). Right panel: steady-state fitting of equilibrium responses and  $K_D$  calculation on the basis of the 1:1 binding model. (B–D) SPR sensorgrams showing compound binding ( $>4$  RU) at concentrations of 10 (red) or 40  $\mu\text{M}$  (green) to immobilized 6  $\times$  HisMBP-SREBP-1a (1–198) (B,C) or to immobilized 6  $\times$  HisMBP (D). (E) Upper panel: SPR sensorgram showing dose-dependent compound binding (Compound 1 = 3.125, 6.25, 12.5, 25, and 50  $\mu\text{M}$ ; Compound 2 = 12.5, 25, 50, 100, and 200  $\mu\text{M}$ ) to immobilized 6  $\times$  HisMBP-SREBP-1a (1–198). Lower panel: the steady-state fitting of the equilibrium responses and the  $K_D$  calculation on the basis of the 1:1 binding model.

peak of the melt curve; however, the  $T_m$  value of MBP was reported to be around 55  $^\circ\text{C}$ , which is close to that of 6  $\times$  HisMBP-SREBP-1a (1–198).<sup>24</sup> Therefore, the  $T_m$  value of SREBP-1a (1–198) is expected to be similar to that of MBP.

Taken together, we inferred that the MBP tag does not induce a conformational change in the target protein, and the counter assay using purified 6  $\times$  HisMBP could effectively eliminate binders to the MBP tag. This notion is supported by the fact

Table 1. Information on Hit Compounds Identified as SREBP-1 Binders

	IUPAC name	$K_D$ ( $\mu\text{M}$ )	$R_{\text{max}}$ (RU)	Structure
<b>Compound 1</b>	9-phenyl-8,10-dioxatricyclo[7.3.1.02,7]trideca-2,4,6-trien-5-ol	2.44	11.4	
<b>Compound 2</b>	(5E)-5-[1-(1,3-benzodioxol-5-ylmethylamino)propylidene]-1-cyclohexyl-hexahydropyrimidine-2,4,6-trione	56.4	7.46	

that the TSA counter assay using  $6 \times$  HisMBP mostly excluded compounds that showed positive  $T_m$  shifts (Figure 4G). Thus, it is reasonable to consider that hit compounds from the first screening with positive  $T_m$  shifts may bind to MBP, whereas those with negative  $T_m$  shifts may bind to SREBP-1a.

Although TSA enables HTS of binders to target proteins, it cannot guarantee binding specificity or quantitatively evaluate affinity. Therefore, we employed the Biacore T200 instrument to perform SPR analysis to validate the compound-binding capacity and specificity with greater accuracy.<sup>25</sup> Purified  $6 \times$  HisMBP-SREBP-1a (1–198) was immobilized on a CM5 sensor chip using an amine-coupling kit. As the isoelectric point of the purified protein was between 4.5 and 4.6, we preconcentrated the protein at a lower pH of 4.4 and optimized the conditions for the immobilization of SREBP-1 on the CM5 surface. Approximately 7000 resonance units (RU) of the proteins were immobilized. To confirm the conformationally active state of the immobilized protein, we determined the dose-dependent binding response and dissociation constant ( $K_D$ ), an affinity indicator, of maltose (at concentrations from 0.1 to 100  $\mu\text{M}$ ) against  $6 \times$  HisMBP-SREBP-1a (1–198). The results indicated that the maximum binding response ( $R_{\text{max}}$ ) and  $K_D$  values were 15.8 RU and 1.33  $\mu\text{M}$ , respectively (Figure 5A). Considering that the  $K_D$  of maltose against MBP is reported to be approximately 2  $\mu\text{M}$ , it was implied that  $6 \times$  HisMBP-SREBP-1a (1–198) maintains its conformation and that SPR analysis functions properly. On the basis of the results of our screening, we examined the binding capacities of the 78 compounds selected using TSA. These compounds were diluted in running buffer containing 2% DMSO and injected into the sensor chip at final concentrations of 10 and 40  $\mu\text{M}$ . Of these, 21 compounds showed binding responses of more than four RU (Figures 5B). However, the  $R_{\text{max}}$  values of the two compounds exceeded three times the calculated  $R_{\text{max}}$  values, thereby suggesting that they were nonspecific binders and were, therefore, eliminated as false positive compounds (Figure 5C). We then immobilized  $6 \times$  HisMBP-FLAG, which excludes SREBP-1a, on the CM5 sensor chip and evaluated the binding responses of the selected compounds at final concentrations of 10 and 40  $\mu\text{M}$ . Nine compounds with binding responses over four RU were excluded because they were regarded as not targeting SREBP-1a (Figures 5D). The 12 remaining compounds were subjected to dose-dependent analysis (from 3.125 to 50  $\mu\text{M}$ ),

and the two compounds exhibited a dose-dependent binding response (Figure 5E). Compound 2 did not show clear saturation at lower concentrations; therefore, a dose-dependent assay was performed up to a concentration of 200  $\mu\text{M}$ , which showed a saturation-binding signal. On the basis of these results, we conclude that these compounds are novel SREBP-1a binders. The structures and IUPAC names of the hit compounds, along with their  $R_{\text{max}}$  and  $K_D$  values, are listed in Table 1. While there are no reports on Compound 1, according to PubChem search results, Compound 2 was reported to function as an inhibitor of the T-Type Calcium Channel with an  $EC_{50}$  value of 5.15  $\mu\text{M}$  (BioAssay AID: 489005), although the  $K_D$  value of Compound 2 for SREBP-1 (1–198) deviated from its  $EC_{50}$  value by more than 10-fold.

As a next step, compound properties, including physical properties, affinity, and specificity, should be improved through structure–activity relationships (SAR) prior to in vitro cell-based assays followed by in vivo examination. Possible cell-based assays include examining the inhibitory effects of the optimized compounds on the expression levels of SREBP-1 target genes and proteolytic activation of SREBP-1 in human cells that express SREBP-1, such as hepatocytes. If labeled binders can be synthesized, it will be possible to conduct a pull-down assay against endogenous SREBP-1 to ensure that binders against SREBP-1 (1–198) can bind to endogenous SREBP-1. Although the amino acid sequence homology between SREBP-1 and SREBP-2 in the N-terminal region of 1–198 is approximately 30.7%, which is low compared with 46% of the total amino acid sequence, evaluation of the selectivity against SREBP-2 would be required for the compounds to be developed into drugs.

Isothermal titration calorimetry (ITC) may be a promising tool for analyzing compound SAR,<sup>26</sup> given the lack of a solved protein structure for human SREBP-1. ITC can distinguish enthalpy-driven bonds, such as hydrogen bonds and van der Waals forces, from entropy-driven bonds, such as hydrophobic interactions, in the binding contributions. The enthalpy-driven thermodynamic signature reflects specific binding to the target protein, which is useful for optimizing compound structures.<sup>27</sup> Additionally, the presence of binding pockets in SREBP-1, in which small molecules regulate their activity, remains unknown. If SREBP-1 binders have little impact on its activity, protein knockdown technology, which can degrade the target

proteins of interest through the ubiquitin-proteasome pathway, may offer a promising alternative approach.<sup>28</sup>

Our research led to the identification of novel human SREBP-1 binders using purified recombinant proteins. The application of purified SREBP-1 may provide insights into its protein structure and compound-binding sites, which would facilitate the investigation of structure–activity relationships among hit compounds. Additionally, our findings suggest the potential of purifying the N-terminal region of human SREBP-2, which could contribute to the understanding of the structural differences between SREBP-1 and SREBP-2 and determine the binding selectivity of the compounds. The development of SREBP-1-specific inhibitors would enable examination of the proof-of-concept of SREBP-1 as a therapeutic target molecule with ease and precision, both in vitro and in vivo. Furthermore, these inhibitors could serve as lead compounds for potential therapeutic drugs.

## ■ ASSOCIATED CONTENT

### SI Supporting Information

The Supporting Information is available free of charge at <https://pubs.acs.org/doi/10.1021/acsmmedchemlett.4c00067>.

Materials and methods (compound library, expression and purification of SREBP-1, SDS-PAGE, CBB staining, immunoblotting, TSA) and additional references (PDF)

## ■ AUTHOR INFORMATION

### Corresponding Authors

**Yu Takahashi** – Food Biochemistry Laboratory, Department of Applied Biological Chemistry, Graduate School of Agricultural and Life Sciences, The University of Tokyo, Tokyo 113-8657, Japan; [orcid.org/0000-0003-3186-2925](https://orcid.org/0000-0003-3186-2925); Email: [ayutaka@g.ecc.u-tokyo.ac.jp](mailto:ayutaka@g.ecc.u-tokyo.ac.jp)

**Ryuichiro Sato** – Nutri-Life Science Laboratory, Department of Applied Biological Chemistry, Graduate School of Agricultural and Life Sciences, The University of Tokyo, Tokyo 113-8657, Japan; Email: [roysato@g.ecc.u-tokyo.ac.jp](mailto:roysato@g.ecc.u-tokyo.ac.jp)

### Authors

**Takashi Maruyama** – Food Biochemistry Laboratory, Department of Applied Biological Chemistry, Graduate School of Agricultural and Life Sciences, The University of Tokyo, Tokyo 113-8657, Japan

**Kahori Hiro** – Food Biochemistry Laboratory, Department of Applied Biological Chemistry, Graduate School of Agricultural and Life Sciences, The University of Tokyo, Tokyo 113-8657, Japan

**Kohji Murase** – The Bioorganic Chemistry Laboratory, Department of Applied Biological Chemistry, Graduate School of Agricultural and Life Sciences, The University of Tokyo, Tokyo 113-8657, Japan

**Hirotatsu Kojima** – Drug Discovery Initiative, Graduate School of Pharmaceutical Sciences, The University of Tokyo, Tokyo 113-0033, Japan; [orcid.org/0000-0002-5480-3189](https://orcid.org/0000-0002-5480-3189)

**Takayoshi Okabe** – Drug Discovery Initiative, Graduate School of Pharmaceutical Sciences, The University of Tokyo, Tokyo 113-0033, Japan

**Yoshio Yamauchi** – Food Biochemistry Laboratory, Department of Applied Biological Chemistry, Graduate

School of Agricultural and Life Sciences, The University of Tokyo, Tokyo 113-8657, Japan

Complete contact information is available at:

<https://pubs.acs.org/doi/10.1021/acsmmedchemlett.4c00067>

### Author Contributions

#T.M. and Y.T. contributed equally to this work. Conceptualization, Y.T.; methodology, T.M., Y.T., and K.M.; formal analysis, T.M., Y.T., and K.H.; investigation, T.M., Y.T., and K.H.; resources, H.K., and T.O.; writing, T.M. and Y.T.; supervision, Y.T. and R.S.; project administration, Y.T., Y.Y., and R.S.; funding acquisition, Y.T. and R.S. All authors approved the final version of the manuscript.

### Funding

This study was supported by the Ministry of Education, Culture, Sports, Science, and Technology of Japan under Grant-in-Aid for Scientific Research A (20H00408 to R.S.) and Grant-in-Aid for Scientific Research C (23K05070 to Y.T.) and Basis for Supporting Innovative Drug Discovery and Life Science Research from AMED under Grant Number JP22ama121053 (support number 1470).

### Notes

The authors declare no competing financial interest.

## ■ ACKNOWLEDGMENTS

We thank Drs. Riyo Imamura, Takuya Ikeda, and Kosuke Yasuda for technical support and helpful discussions.

## ■ ABBREVIATIONS

6 × His, hexahistidine; AAs, amino acids; AR, androgen receptor; IPTG,  $\beta$ -D-thiogalactopyranoside; CBB, Coomassie brilliant blue;  $\Delta T_m$ ,  $T_m$  shift values; HTS, high-throughput screening; INSIG, insulin-induced gene protein; ITC, isothermal titration calorimetry;  $K_D$ , dissociation constant; MBP, maltose-binding protein; PAGE, polyacrylamide gel electrophoresis;  $R_{max}$ , maximum binding response; RU, resonance units; SAR, structure–activity relationships; SCAP, SREBP cleavage-activating protein; SDS, sodium dodecyl sulfate; SREBP, sterol regulatory element-binding protein; SD, standard deviation; SPR, surface plasmon resonance;  $T_m$ , melting temperature; TSA, thermal shift assay

## ■ REFERENCES

- (1) Fahed, G.; Aoun, L.; Zerdan, M. B.; Allam, S.; Zerdan, M. B.; Bouferraa, Y.; Assi, H. I. Metabolic Syndrome: Updates on Pathophysiology and Management in 2021. *Int. J. Mol. Sci.* **2022**, *23* (2), 786.
- (2) Yokoyama, C.; Wang, X.; Briggs, M. R.; Admon, A.; Wu, J.; Hua, X.; Goldstein, J. L.; Brown, M. S. SREBP-1, a Basic-Helix-Loop-Helix-Leucine Zipper Protein That Controls Transcription of the Low Density Lipoprotein Receptor Gene. *Cell* **1993**, *75* (1), 187–197.
- (3) Takahashi, Y.; Shinoda, A.; Furuya, N.; Harada, E.; Arimura, N.; Ichi, I.; Fujiwara, Y.; Inoue, J.; Sato, R. Perilipin-Mediated Lipid Droplet Formation in Adipocytes Promotes Sterol Regulatory Element-Binding Protein-1 Processing and Triacylglyceride Accumulation. *PLoS One* **2013**, *8*, No. e64605.
- (4) Shimomura, I.; Matsuda, M.; Hammer, R. E.; Bashmakov, Y.; Brown, M. S.; Goldstein, J. L. Decreased IRS-2 and Increased SREBP-1c Lead to Mixed Insulin Resistance and Sensitivity in Livers of Lipodystrophic and Ob/Ob Mice. *Mol. Cell* **2000**, *6* (1), 77–86.
- (5) Shimano, H.; Shimomura, I.; Hammer, R. E.; Herz, J.; Goldstein, J. L.; Brown, M. S.; Horton, J. D. Elevated Levels of SREBP-2 and Cholesterol Synthesis in Livers of Mice Homozygous for a Targeted

Disruption of the SREBP-1 Gene. *J. Clin. Invest.* **1997**, *100* (8), 2115–2124.

(6) Shimano, H.; Sato, R. SREBP-Regulated Lipid Metabolism: Convergent Physiology-Divergent Pathophysiology. *Nat. Rev. Endocrinol.* **2017**, *13* (12), 710–730.

(7) Yan, R.; Cao, P.; Song, W.; Li, Y.; Wang, T.; Qian, H.; Yan, C.; Yan, N. Structural Basis for Sterol Sensing by Scap and Insig. *Cell Rep.* **2021**, *35* (13), 109299.

(8) Tang, J.-J.; Li, J.-G.; Qi, W.; Qiu, W.-W.; Li, P.-S.; Li, B.-L.; Song, B.-L. Inhibition of SREBP by a Small Molecule, Betulin, Improves Hyperlipidemia and Insulin Resistance and Reduces Atherosclerotic Plaques. *Cell Metab.* **2011**, *13* (1), 44–56.

(9) Kamisuki, S.; Mao, Q.; Abu-Elheiga, L.; Gu, Z.; Kugimiya, A.; Kwon, Y.; Shinohara, T.; Kawazoe, Y.; Sato, S.; Asakura, K.; Choo, H.-Y. P.; Sakai, J.; Wakil, S. J.; Uesugi, M. A Small Molecule That Blocks Fat Synthesis by Inhibiting the Activation of SREBP. *Chem. Biol.* **2009**, *16* (8), 882–892.

(10) Zheng, Z. G.; Zhu, S. T.; Cheng, H. M.; Zhang, X.; Cheng, G.; Thu, P. M.; Wang, S. P.; Li, H. J.; Ding, M.; Qiang, L.; Chen, X. W.; Zhong, Q.; Li, P.; Xu, X. Discovery of a Potent SCAP Degrader That Ameliorates HFD-Induced Obesity, Hyperlipidemia and Insulin Resistance via an Autophagy-Independent Lysosomal Pathway. *Autophagy* **2021**, *17* (7), 1592–1613.

(11) Suzuki, R.; Ferris, H. A.; Chee, M. J.; Maratos-Flier, E.; Kahn, C. R. Reduction of the Cholesterol Sensor SCAP in the Brains of Mice Causes Impaired Synaptic Transmission and Altered Cognitive Function. *PLoS Biol.* **2013**, *11* (4), No. e1001532.

(12) Amemiya-Kudo, M.; Shimano, H.; Hasty, A. H.; Yahagi, N.; Yoshikawa, T.; Matsuzaka, T.; Okazaki, H.; Tamura, Y.; Iizuka, Y.; Ohashi, K.; Osuga, J.; Harada, K.; Gotoda, T.; Sato, R.; Kimura, S.; Ishibashi, S.; Yamada, N. Transcriptional Activities of Nuclear SREBP-1a, -1c, and -2 to Different Target Promoters of Lipogenic and Cholesterogenic Genes. *J. Lipid Res.* **2002**, *43* (8), 1220–1235.

(13) Zhang, R.; Monsma, F. Fluorescence-Based Thermal Shift Assays. *Curr. Opin. Drug Discov. Devel.* **2010**, *13* (4), 389–402.

(14) Wang, J.; Wang, Q.; Song, S. Research Progress of Surface Plasmon Resonance Technology in Drug Discovery. *J. Chin. Pharm. Sci.* **2020**, *29* (7), 504.

(15) Urner, L. H.; Junge, F.; Fiorentino, F.; El-Baba, T. J.; Shutin, D.; Nölte, G.; Haag, R.; Robinson, C. V. Rationalizing the Optimization of Detergents for Membrane Protein Purification. *Chem.—Eur. J.* **2023**, *29* (30), No. e202300159.

(16) Denisov, I. G.; Sligar, S. G. Nanodiscs for Structural and Functional Studies of Membrane Proteins. *Nat. Struct. Mol. Biol.* **2016**, *23*, 481–486.

(17) Birkholtz, L. M.; Blatch, G.; Coetzer, T. L.; Hoppe, H. C.; Human, E.; Morris, E. J.; Ngcete, Z.; Oldfield, L.; Roth, R.; Shonhai, A.; Stephens, L.; Louw, A. I. Heterologous Expression of Plasmodial Proteins for Structural Studies and Functional Annotation. *Malar. J.* **2008**, *7*, 197.

(18) Raran-Kurussi, S.; Waugh, D. S. The Ability to Enhance the Solubility of Its Fusion Partners Is an Intrinsic Property of Maltose-Binding Protein but Their Folding Is Either Spontaneous or Chaperone-Mediated. *PLoS One* **2012**, *7* (11), e49589.

(19) Buchan, D. W. A.; Jones, D. T. The PSIPRED Protein Analysis Workbench: 20 Years On. *Nucleic Acids Res.* **2019**, *47* (W1), W402–W407.

(20) Rishi, V.; Gal, J.; Krylov, D.; Fridriksson, J.; Boysen, M. S.; Mandrup, S.; Vinson, C. SREBP-1 Dimerization Specificity Maps to Both the Helix-Loop-Helix and Leucine Zipper Domains: Use of a Dominant Negative. *J. Biol. Chem.* **2004**, *279* (12), 11863–11874.

(21) Gao, K.; Oerlemans, R.; Groves, M. R. Theory and Applications of Differential Scanning Fluorimetry in Early-Stage Drug Discovery. *Biophys. Rev.* **2020**, *12* (1), 85–104.

(22) Kean, J.; Cleverley, R. M.; O’Ryan, L.; Ford, R. C.; Prince, S. M.; Derrick, J. P. Characterization of a CorA Mg<sup>2+</sup> Transport Channel from *Methanococcus Jannaschii* Using a Thermofluor-Based Stability Assay. *Mol. Membr. Biol.* **2008**, *25* (8), 653–663.

(23) Yamanaka, K.; Takahashi, Y.; Azuma, Y.; Hantani, Y. Assay Development and Screening for the Identification of Ganglioside GM3 Synthase Inhibitors. *Biochemistry* **2020**, *59* (12), 1242–1251.

(24) Bai, N.; Roder, H.; Dickson, A.; Karanicolas, J. Isothermal Analysis of ThermoFluor Data Can Readily Provide Quantitative Binding Affinities. *Sci. Rep.* **2019**, *9* (1), 2650.

(25) Genick, C. C.; Barlier, D.; Monna, D.; Brunner, R.; Bé, C.; Scheufler, C.; Ottl, J. Applications of Biophysics in High-Throughput Screening Hit Validation. *J. Biomol. Screen.* **2014**, *19* (5), 707.

(26) Cimperman, P.; Baranauskienė, L.; Jachimovičiūtė, S.; Jachno, J.; Torresan, J.; Michailoviene, V.; Matuliene, J.; Sereikaite, J.; Bumelis, V.; Matulis, D. A Quantitative Model of Thermal Stabilization and Destabilization of Proteins by Ligands. *Biophys. J.* **2008**, *95* (7), 3222–3231.

(27) Yin, F.; Cao, R.; Goddard, A.; Zhang, Y.; Oldfield, E. Enthalpy versus Entropy-Driven Binding of Bisphosphonates to Farnesyl Diphosphate Synthase. *J. Am. Chem. Soc.* **2006**, *128* (11), 3524–3525.

(28) Békés, M.; Langle, D. R.; Crews, C. M. PROTAC Targeted Protein Degradation: The Past Is Prologue. *Nat. Rev. Drug Discov.* **2022**, *21*, 181–200.